Multistep navigation of leukocytes: a stochastic model with memory effects

Dietmar Oelz[*], Christian Schmeiser[†*] and Alexander Soreff[*]

August 7, 2005

Acknowledgement: This work has been supported by the *Wittgenstein 2000* Award of P.Markowich, the *Wittgenstein 1998* Award of W. Schachermayer, the European network 'Hyperbolic and Kinetic Equations' (HYKE) and by the Austrian Science Fund (FWF) Wissenschaftskolleg *Differential Equations*.

Abstract

We present a model for the chemotactically directed migration of neutrophil leukocytes. It reproduces the multistep navigation by memory effects investigated experimentally by E.F. Foxman, J.J. Campbell, and E.C. Butcher in [Foxman, Campbell and Butcher 1997].

The model consists of a system of stochastic differential equations. The long time behaviour of the corresponding deterministic system is analysed and two approaches for the numerical solution of the full stochastic system are compared. One of them consists in performing direct simulations, the other one is based on a moment approximation of the Fokker-Planck equation and numerical methods for convection dominated partial differential equations (PDEs).

Key words: Chemotaxis, Leukocytes.

1 Introduction

In the course of an inflammatory process leukocytes are attracted by messenger substances (chemoattractants) to the location of inflammation in order to fight microbes and to remove debris (cp. [Goldsby, Kindt, Osborne and Kuby 2000]).
In 1997, E.F. Foxman, J.J. Campbell and E. C. Butcher ([Foxman, Campbell and Butcher 1997]) published experimental results on the migration of neutrophils being exposed to two different chemoattractants.

They found that leukocytes follow the gradients of chemoattractants rather than their mere concentration. Furthermore they found evidence that neutrophils can migrate down a local gradient towards a distant source of chemoattractant. They established the hypothesis that this behaviour "reflects a more

[*]Institute for Analysis und Scientific Computing. Vienna Univ. of Technology, Wiedner Hauptstr. 8-10, A-1040 Wien, Austria

[†]Johann Radon Institute for Computational and Applied Mathematics (RICAM), Linz

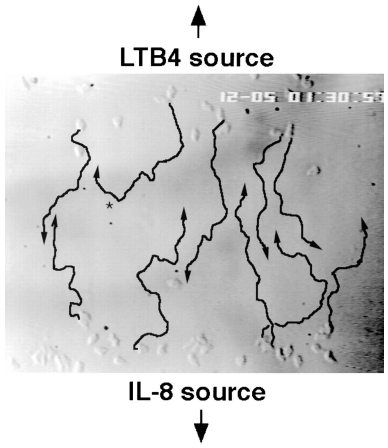

Figure 1: Time-lapse video microscopy taken from [Foxman, Campbell and Butcher 1997], cells are exposed to the two chemoattractants Leukotriene B4 (LTB4) and Interleukin-8 (IL-8) and the migration paths of representative cells are recorded during 15 minutes.

efficient or rapid adaption of the migrating cell to increasing vs. decreasing attractant concentrations." They even found experimental evidence that tightly neighbouring cells may migrate in opposite directions though they share the same surroundings (see figure 1).

Motivated by these results we develop a mathematical model to describe this behaviour. We denote the position of one single cell by

$$\boldsymbol{x}(t) := (x(t), y(t)) \in \mathbb{R}^2 \, .$$

Furthermore we assume the presence of m chemoattractant substances. We denote their concentrations by $S_i(\boldsymbol{x})$, $1 \leq i \leq m$ and assume that these functions are given and that they are stationary, which does not affect the qualitative properties of the model. In general, however, diffusion, production, and decay of chemoattractants should be considered.

Every single cell has receptors which let the cell perceive the directions and strengths of chemoattractant gradients. According to the experimental data (see [Foxman, Campbell and Butcher 1997]) we assume that each cell has a dynamically changing sensitivity $\chi_i(t) \geq 0$ for the chemoattractant S_i, $1 \leq i \leq m$. These represent the responsiveness of cells to the presence of the respective chemoattractant gradient, which depends, among other things, on the absolute number of receptors for the respective chemoattractant and on the number of "free" receptors, i.e. on the fraction of receptors which are not bound to a chemoattractant molecule.

As an expression for the speed of migration we therefore sum up the contributions $\chi_i \nabla S_i$. This leads to a deterministic equation for the evolution of the spatial position of a single leukocyte,

$$\dot{\boldsymbol{x}}(t) = \sum_{i=1}^{m} \chi_i(t) \nabla S_i(\boldsymbol{x}(t)) \, . \tag{1.1}$$

Observe that with respect to their function and physical dimension, the sensitivities χ_i correspond to the notion of sensitivity used in the Patlak-Keller-

Segel-Model for chemotaxis. Experimental behaviour (see [Foxman, Campbell and Butcher 1997]) indicates that the sensitivity for a chemoattractant is downregulated in situations where the concentration of this chemoattractant is high. For that reason we assume that for each sensitivity χ_i the vector $S := (S_1, \ldots, S_m)^T$ of chemoattractant concentrations is mapped to some target value in the interval $[\chi_i^{\min}, \chi_i^{\max}]$. The target values are

$$\hat{\chi}_i(S) := \chi_i^{\min} + \frac{1}{(AS)_i + \frac{1}{\chi_i^{\max} - \chi_i^{\min}}}, \quad i = 1, \ldots, m\,, \tag{1.2}$$

where $A = (a_{ij})_{1 \le i,j \le m}$, $a_{ij} \ge 0$ is the matrix of downregulation factors. In the case where sensitivities are only downregulated by their associated chemoattractants, it is a diagonal matrix. We may use non-diagonal entries to model dominating chemoattractants which have the ability to downregulate sensitivities even for other chemoattractants. Experiments reflecting this phenomenon can be found in [Foxman, Campbell and Butcher 1997].

The alternative to (1.2), $\hat{\chi}_i(S) := \chi_i^{\min} + 1/\big((AS)_i + (\chi_i^{\max} - \chi_i^{\min})^{-\frac{1}{2}}\big)^2$, has been used in [Oelz and Schmeiser 2004], where we perform simulations of experiments in [Foxman, Campbell and Butcher 1997]. Both expressions can be derived from discrete random walks (see [Painter, Maini and Othmer 2000]).

Observe that $\chi_i^{\min}$ is the minimal sensitivity, which is reached when downregulation is maximal. In general this will be the case when the concentration of the associated chemoattractant is very high. $\chi_i^{\max}$, on the other hand, represents the maximum level of sensitivity of the cell. The actual sensitivity will be close to $\chi_i^{\max}$ at points where there is hardly any chemoattractant.

Our main modelling contribution is the assumption that the sensitivities do not adapt immediately to the local values of the chemoattractant concentrations. Instead their dynamics is determined by the relaxation model

$$\dot{\chi}_i(t) = \alpha_i(\hat{\chi}_i(S(\boldsymbol{x}(t))) - \chi_i(t))\,, \tag{1.3}$$

where $\alpha_i > 0$ is the rate of adaption of the sensitivity χ_i to its target value.

It would be unrealistic to expect leukocytes to behave completely deterministically. Therefore we modify the system (1.1)-(1.3) to a system of stochastic differential equations to describe the time dependent state of one single leukocyte. Thus, we consider a stochastic process

$$X(t) := \begin{pmatrix} \boldsymbol{x}(t) \\ \chi_1(t) \\ \vdots \\ \chi_m(t) \end{pmatrix}$$

in the state space $\mathbb{R}^2 \times [\chi_1^{\min}, \chi_1^{\max}] \times \ldots \times [\chi_m^{\min}, \chi_m^{\max}]$, determined by the stochastic differential equation (SDE)

$$dX = \mathbf{b}(X)dt + \Sigma\, dB, \quad \text{where} \tag{1.4}$$

$$\mathbf{b}(\boldsymbol{x}, \chi_1, \ldots, \chi_m) := \begin{pmatrix} \sum_{i=1}^m \chi_i \nabla S_i(\boldsymbol{x}) \\ \alpha_1(\hat{\chi}_1(S(\boldsymbol{x})) - \chi_1) \\ \vdots \\ \alpha_m(\hat{\chi}_m(S(\boldsymbol{x})) - \chi_m) \end{pmatrix}, \quad \Sigma := \begin{pmatrix} \sigma & 0 \\ 0 & \sigma \\ 0 & 0 \\ \vdots & \vdots \\ 0 & 0 \end{pmatrix}, \tag{1.5}$$

$$dB := \begin{pmatrix} dB^x \\ dB^y \end{pmatrix},$$

and $\sigma > 0$. The drift vector $\mathbf{b}(X)$ reflects the deterministic model, and the (constant) volatility matrix Σ creates some randomness in the evolution of the spatial components. By B^x and B^y we denote independent identically distributed nomalised Brownian motions. Refer to [Ionides, Fang, Isseroff and Oster 2004] for another application of SDEs in modelling cell motion.

We scale the problem with respect to typical values of the variables. Let D be the average distance between sources of chemoattractant. Let $\langle S_i \rangle$ be some average value of the chemoattractant concentration S_i on the domain. We furthermore introduce the average (scalar) chemotactic velocity V of one cell. Finally let $\langle \alpha \rangle$ be an average value of the coefficients α_i. Then we introduce the following scaling,

$$\tilde{t} = t\langle \alpha \rangle, \quad \tilde{\boldsymbol{x}} = \frac{\boldsymbol{x}}{D}, \quad \tilde{S}_i = \frac{S_i}{\langle S_i \rangle}, \quad \tilde{\chi}_i = \frac{\chi_i \langle S_i \rangle}{VD}, \quad d\tilde{B} = dB\sqrt{\langle \alpha \rangle}$$

$$\tilde{\alpha}_i = \frac{\alpha_i}{\langle \alpha \rangle}, \quad \tilde{\chi}_i^{\min,\,\max} = \frac{\chi_i^{\min,\,\max} \langle S_i \rangle}{VD}, \quad \tilde{a}_{ij} = V\,D \frac{\langle S_j \rangle}{\langle S_i \rangle} a_{ij}, \quad \tilde{\sigma} = \frac{\sigma}{D\sqrt{\langle \alpha \rangle}},$$

and rewrite the system (1.4), but stay with the old expressions for the scaled quantities

$$dX = \mathbf{b}(X)dt + \Sigma\, dB, \quad \text{where} \tag{1.6}$$

$$\mathbf{b}(\boldsymbol{x}, \chi_1, \ldots, \chi_m) := \begin{pmatrix} \frac{1}{\varepsilon} \sum_{i=1}^{m} \chi_i \nabla S_i(\boldsymbol{x}) \\ \alpha_1 \Big(\hat{\chi}_1(S(\boldsymbol{x})) - \chi_1 \Big) \\ \vdots \\ \alpha_m \Big(\hat{\chi}_m(S(\boldsymbol{x})) - \chi_m \Big) \end{pmatrix},$$

with $\hat{\chi}_i(S)$, Σ and dB as in (1.5), (1.2). The dimensionless parameter

$$\varepsilon := \frac{\langle \alpha \rangle D}{V}$$

is the ratio of the mean migration time between two sources of chemoattractant to the relaxation time of the sensitivities.

For the rest of the paper we restrict ourselves to the case of two chemoattractants, i.e. $m = 2$. In Section 2 the long time behaviour of the corresponding deterministic system is analysed by considering special choices for the functions $\hat{\chi}_i(S)$ and $S_i(\boldsymbol{x})$. It is shown that the memory effect in our model may lead to oscillations of cells between the chemoattractant centres. In Section 3, a macroscopic model is derived by a moment expansion of the Fokker-Planck equation corresponding to (1.6). The macroscopic model is a system of parabolic equations for the cell density and the mean values of the chemotactic sensitivities. Numerical approaches to the solution of the SDE system and to the macroscopic model are presented in Section 4. Finally the results of numerical experiments and comparisons between the models are the content of Section 5.

The main goal of this work is to highlight the basic qualitative properties of the models reflected in their long time behaviour.

2 Deterministic dynamics

To study the dynamics, a simplified model is used. One difference to the biologically more accurate model presented in the introduction lies in the sensitivity functions $\hat{\chi}_i$. They are chosen as $\hat{\chi}_i = 1/S_i$, which corresponds to a special case of the sensitivity equation (1.2), obtained by setting $A = I$, $\alpha_i = 1$, $\chi_{min} = 0$ and $\chi_{max} = \infty$. More importantly, we only study the deterministic model, equations (1.1), (1.3), for two chemoattractants.

We assume that the concentrations of the chemoattractants are given by Gaussians centred around fixed points $\boldsymbol{x}_1 = (x_1, 0)$ and $\boldsymbol{x}_2 = (x_2, 0)$:

$$S_i(\boldsymbol{x}) = \exp\left(\frac{-|\boldsymbol{x} - \boldsymbol{x}_i|^2}{T_i}\right), \quad T_i > 0, \quad i = 1, 2\ . \tag{2.1}$$

The following system of equations is obtained,

$$\begin{aligned} \dot{x} &= \tfrac{1}{\varepsilon}\big(\chi_1 \nabla S_1(\boldsymbol{x}) + \chi_2 \nabla S_2(\boldsymbol{x})\big)\ , \\ \dot{\chi_1} &= \tfrac{1}{S_1(\boldsymbol{x})} - \chi_1\ , \\ \dot{\chi_2} &= \tfrac{1}{S_2(\boldsymbol{x})} - \chi_2\ . \end{aligned} \tag{2.2}$$

The only critical point is given by

$$\begin{pmatrix} x_\infty \\ y_\infty \\ \chi_{1_\infty} \\ \chi_{2_\infty} \end{pmatrix} = \begin{pmatrix} \frac{x_1 T_2 + x_2 T_1}{T_1 + T_2} \\ 0 \\ 1/S_1(x_\infty, y_\infty) \\ 1/S_2(x_\infty, y_\infty) \end{pmatrix}\ . \tag{2.3}$$

Note that $\boldsymbol{x}_\infty$ lies on the line segment connecting $\boldsymbol{x}_1$ and $\boldsymbol{x}_2$. The eigenvalues of the linearised system are

$$\begin{aligned} \lambda_1 &= -\tfrac{2(T_1+T_2)}{\varepsilon T_1 T_2}, & \lambda_2 &= -1, \\ \lambda_3 &= \tfrac{-p}{2} + \sqrt{\tfrac{p^2}{4} - q}, & \lambda_4 &= \tfrac{-p}{2} - \sqrt{\tfrac{p^2}{4} - q}, \end{aligned} \tag{2.4}$$

$$\text{where} \quad p = \frac{2(T_1+T_2)}{\varepsilon T_1 T_2} - \frac{8(x_2 - x_1)^2}{\varepsilon (T_1+T_2)^2} + 1 \quad \text{and} \quad q = \frac{2(T_1+T_2)}{\varepsilon T_1 T_2}$$

While λ_1 and λ_2 are always negative, the pair (λ_3, λ_4) crosses the imaginary axis when p changes sign, and a Hopf bifurcation occurs. As an example, we choose the parameter values (also used in the numerical experiments in Section 5)

$$T_1 = T_2 = 6, \quad x_1 = -2, \quad x_2 = 2 \tag{2.5}$$

whence $p = 1 - \frac{2}{9\varepsilon}$ and ε can be used as bifurcation parameter with the bifurcation point $\varepsilon^* = 2/9$.

The Hopf bifurcation theorem applies since the eigenvalues (λ_3, λ_4) cross the imaginary axis at nonzero speed. Numerical simulations (see Figure 2) suggest that the system has a stable limit cycle for $\varepsilon < 2/9$, hence a supercritical Hopf bifurcation occurs.

The stable limit cycle for strong enough memory effects (small enough ε) reflects the main qualitative property of our model: The cells' ability to migrate away from the location of peak concentration of one chemoattractant by following the chemical gradient of a second chemoattractant with distant source.

For the full stochastic model we expect the existence of an attractive time invariant probability distribution, which is spread out around the limit cycle of the deterministic model. This will be verified by the numerical experiments in section 5.

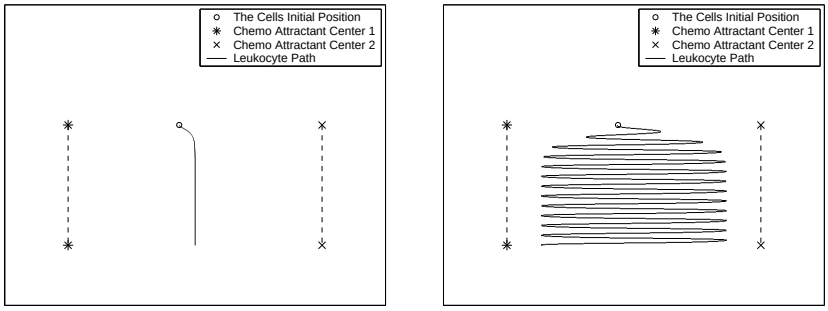

(a) Stable steady state. (b) Stable limit cycle.

Figure 2: *Numerical solution of the deterministic system (2.1), (2.2) with parameter values (2.5) and different values of ε. The horizontal and vertical (downward) directions are the x- and, resp., t-directions.*

3 A macroscopic model

The Fokker-Planck equation (cp. [Œksendal 1995], 'Kolmogorov forward equation') associated to the SDE (1.6) in the case $m = 2$ is the linear partial differential equation (PDE)

$$\frac{\partial g}{\partial t} = \frac{\sigma^2}{2}\Delta_{\boldsymbol{x}} g - \nabla_X \cdot \big(g\mathbf{b}(X)\big) \tag{3.1}$$

for the distribution function $g(t, X) = g(t, x, y, \chi_1, \chi_2)$, which may be interpreted as probability density for the state of one cell or as density of a population of cells. The equation (3.1) is of mixed hyperbolic-parabolic type since diffusion only acts in the position directions.

As a direct numerical approach to (3.1) would be very expensive we apply the technique of *moment expansion* to reduce the four dimensional model to two dimensions by integrating with respect to the sensitivities. Note that (3.1) preserves the property $\operatorname{supp} g \subseteq \mathbb{R}^2 \times [\chi_1^{\min}, \chi_1^{\max}] \times [\chi_2^{\min}, \chi_2^{\max}]$. For any function $f(t, X)$ we therefore define

$$\overline{f}(t, x, y) := \int_{\chi_1^{\min}}^{\chi_1^{\max}} \int_{\chi_2^{\min}}^{\chi_2^{\max}} f(t, x, y, \chi_1, \chi_2)\, d\chi_2 d\chi_1 \ .$$

Then $\overline{g}$ can be viewed as a marginal probability density of one cell or as position density of a population of cells.

By integrating (3.1) with respect to χ_1 and χ_2 we derive

$$\frac{\partial \overline{g}}{\partial t} = \frac{\sigma^2}{2}\Delta \overline{g} - \frac{1}{\varepsilon}\nabla \cdot \Big(\sum_{i=1}^{2} \overline{g\chi_i}\, \nabla S_i\Big) \ , \tag{3.2}$$

where from now on, ∇ and Δ are meant with respect to $\boldsymbol{x}$. Equations for the first order moments $\overline{g\chi_j}$ are derived by multiplying (3.1) by χ_j and integrating as in (3.2):

$$\frac{\partial}{\partial t}(\overline{g\chi_j}) = \frac{\sigma^2}{2}\Delta(\overline{g\chi_j}) - \frac{1}{\varepsilon}\nabla\cdot(\sum_{i=1}^{2}\overline{g\chi_i\chi_j}\,\nabla S_j) + \alpha_j(\hat{\chi}_j(S)\overline{g} - \overline{g\chi_j})\,. \quad (3.3)$$

In these equations the second order moments appear and we are confronted with the standard closure problem. We introduce the positive definite covariance matrix of the two sensitivities

$$C := \begin{pmatrix} c_{11} & c_{12} \\ c_{12} & c_{22} \end{pmatrix},$$

and use the *closure relations*

$$\overline{g\chi_i\chi_j} = \overline{g}\big(c_{ij} + \overline{\chi_i}\,\overline{\chi_j}\big), \quad \text{with} \quad \overline{\chi_i} := \frac{\overline{g\chi_i}}{\overline{g}}\,.$$

The sensitivities are distributed around the expected value, the covariance matrix C representing the "width" of their common distribution. Thus, also in the macroscopic model different values of the sensitivities and, therefore, different chemotactic velocities coexist at one position.

Substituting these expressions into (3.3), we obtain

$$\frac{\partial}{\partial t}(\overline{g}\,\overline{\chi_j}) = \frac{\sigma^2}{2}\Delta(\overline{g}\,\overline{\chi_j}) - \frac{1}{\varepsilon}\nabla\cdot(\sum_{i=1}^{2}\overline{g}\big(c_{ij} + \overline{\chi_i}\,\overline{\chi_j}\big)\,\nabla S_j) + \\ + \alpha_j\,\overline{g}(\hat{\chi}_j(S) - \overline{\chi_j})\,, \quad j = 1,2. \quad (3.4)$$

Note that, by the linearity of the flux $\mathbf{b}$ with respect to χ_1 and χ_2, no further closure assumptions are needed, and (3.2), (3.4) form a closed system of parabolic equations for the density $\overline{g}$ and the expected sensitivities $\overline{\chi}_j$.

We introduce the notation

$$u(t,\boldsymbol{x}) := \begin{pmatrix} \overline{g}(t,\boldsymbol{x}) \\ \overline{g}\,\overline{\chi_1}(t,\boldsymbol{x}) \\ \overline{g}\,\overline{\chi_2}(t,\boldsymbol{x}) \end{pmatrix}$$

and rewrite (3.2) and (3.4) to obtain

$$\frac{\partial}{\partial t}u = \frac{\sigma^2}{2}\Delta u - \frac{1}{\varepsilon}\nabla\cdot\mathbf{f}(u,\boldsymbol{x}) + \Psi(u,\boldsymbol{x})\,, \quad (3.5)$$

with the flux vector $\mathbf{f} = (f^x, f^y)$ and the source term

$$\Psi(u,\boldsymbol{x}) = \begin{pmatrix} 0 \\ \alpha_1\,\overline{g}(\hat{\chi}_1(S(\boldsymbol{x})) - \overline{\chi_1}) \\ \alpha_2\,\overline{g}(\hat{\chi}_2(S(\boldsymbol{x})) - \overline{\chi_2}) \end{pmatrix}\,. \quad (3.6)$$

The fluxes f^x and f^y share the same structure. They differ only insofar as f^x depends on derivatives of the chemoattractants with respect to x whereas

f^y depends on the respective derivatives with respect to y. We therefore look at the generic flux function

$$f^d(u,\boldsymbol{x}) := \begin{pmatrix} \overline{g}\sum_{i=1}^2 \overline{\chi_i} S_{id}(\boldsymbol{x}) \\ \overline{g}\sum_{i=1}^2 \big(c_{i1} + \overline{\chi_i}\,\overline{\chi_1}\big) S_{id}(\boldsymbol{x}) \\ \overline{g}\sum_{i=1}^2 \big(c_{i2} + \overline{\chi_i}\,\overline{\chi_2}\big) S_{id}(\boldsymbol{x}) \end{pmatrix} , \tag{3.7}$$

from which we obtain linear combinations $\alpha f^x + \beta f^y$ by setting $S_{id} = \alpha S_{ix} + \beta S_{iy}$. To implement the numerical method presented in Section 4.2 and to check for hyperbolicity we need the spectral decomposition of the Jacobian $D_u f^d$. We define

$$\omega_d := \sqrt{S_d C S_d^T}, \quad \text{where} \quad S_d := (S_{1d}, S_{2d}) ,$$

which is real because of the positive definiteness of C. Then $D_u f^d$ has the following eigenvalues and associated eigenvectors:

$$\lambda_{1,2} = \sum_{i=1}^2 \overline{\chi_i} S_{id} \pm \omega_d, \quad r_{1,2} = \begin{pmatrix} 1 \\ \overline{\chi_1} \pm \frac{\sum_{i=1}^2 c_{i1} S_{id}}{\omega_d} \\ \overline{\chi_2} \pm \frac{\sum_{i=1}^2 c_{i2} S_{id}}{\omega_d} \end{pmatrix} ,$$

$$\lambda_3 = \sum_{i=1}^2 \overline{\chi_i}\, S_{id}, \quad r_j = \begin{pmatrix} 0 \\ S_{2d} \\ -S_{1d} \end{pmatrix} .$$

The structure is similar to the Euler equations of gas dynamics with the cell velocity λ_3 replacing the gas velocity and with the "speed of sound" ω_d. Also the 1- and 2-fields are genuinely nonlinear, and the 3-field is linearly degenerate.

These observations show the hyperbolicity and well posedness of the system

$$\frac{\partial}{\partial t} u + \frac{1}{\varepsilon} \nabla \cdot \mathbf{f}(u,\boldsymbol{x}) = 0 , \tag{3.8}$$

whose solution will be part of an operator splitting approach to (3.5) in Section 4.2. There we also use another structural property of the flux functions, their homogeneity in the sense that they satisfy $f^d(\alpha u, \boldsymbol{x}) = \alpha f^d(u,\boldsymbol{x})$ for any scalar α, which implies Euler's identity

$$f^d(u,\boldsymbol{x}) = D_u f^d(u,\boldsymbol{x}) u . \tag{3.9}$$

4 Numerical methods

4.1 Direct simulation of the microscopic equations

For the numerical solution of the stochastic differential equation (1.6) a semi implicit Euler scheme is used. It is a strong approximation method and thanks to the additive noise of order one, see [Kloeden and Platen 1992] for details.

For computational simplicity the differential equations for the chemotactic sensitivities χ_1 and χ_2 are discretised semi-implicitly with the positions evaluated at the old time step:

$$\frac{\chi_i^{n+1} - \chi_i^n}{\Delta t} = \frac{1}{S_i(\boldsymbol{x}^n)} - \chi_i^{n+1} \qquad i = 1, 2 \; . \tag{4.1}$$

Discretisation of the continuous Brownian motion comes naturally from its definition. Replacing the infinitesimal increment dt by a finite time interval of length Δt, dB is approximated by $\Delta B = \sqrt{\Delta t}(N_1, N_2)$, where $N_1,\ N_2\ iid\ \sim N(0,1)$, meaning that they are two independent normally distributed random variables with zero expectation and variance equal to one.

The difference equations for the stochastic spatial position are fully implicit and take the following form:

$$\frac{\boldsymbol{x}^{n+1} - \boldsymbol{x}^n}{\Delta t} = \frac{\chi_1^{n+1}}{\varepsilon} \nabla S_1(\boldsymbol{x}^{n+1}) + \sigma \Delta B \; . \tag{4.2}$$

At every time step a nonlinear algebraic system for the new position has to be solved.

Probability density approximations are obtained by computing many paths while recording the cells positions in a spatial grid.

4.2 Numerical method for the macroscopic equation

We use the fractional step method (see [Leveque 2002], p. 380) to deal with the evolution of the solution of (3.5) with 4 substeps according to the terms on the right hand side. In particular we use a rectangular grid and treat the fluxes in x-direction and y-direction independently, a strategy which is called dimensional splitting.

- For the diffusion problem, $\frac{\partial u_1}{\partial t} = \frac{\sigma^2}{2} \Delta u_1$, we use the Crank-Nicolson scheme.
- For the transport problems, $\frac{\partial u_2}{\partial t} + \frac{\partial f^x(u_2, \boldsymbol{x})}{\partial x} = 0$ and $\frac{\partial u_3}{\partial t} + \frac{\partial f^y(u_3, \boldsymbol{x})}{\partial y} = 0$, we use the upwind scheme with a high resolution correction. The correction is based on a specific flux vector splitting which makes use of (3.9) (see [Leveque 2002], "Method by Steger and Warming").
- For the reaction problem, $\frac{\partial u_4}{\partial t} = \Psi(u_4, \boldsymbol{x})$, we use the implicit Euler scheme.

5 Numerical experiments

In order to compare the results obtained by the two different models, we compare the steady state solutions with parameters chosen such that the deterministic system has a stable limit cycle.

We consider an equidistant grid with 361×121 grid points on the spatial domain $[-3, 3] \times [-1, 1]$ and use the functions S_1 and S_2 from (2.1) together with (2.5). Furthermore we choose the following values for the scaled model

(1.6)

$$\sigma = \sqrt{5}/3, \quad \alpha_1 = \alpha_2 = 1, \quad A := \begin{pmatrix} 1 & 0 \\ 0 & 1 \end{pmatrix},$$
$$\chi_1^{\max} = \chi_2^{\max} = \infty, \quad \chi_1^{\min} = \chi_2^{\min} = 0,$$
$$\varepsilon = 0.12 < \frac{2}{9} = \varepsilon^*$$

, which equal those of the analysis in Section 2.

To obtain the steady state solution of the microscopic equations, one Leukocyte is started on the deterministic limit cycle and at each time step its position is recorded with respect to a grid. The simulation time depends on the required smoothness. At the end of the simulation the computed density is normalised to obtain a probability density.

The results of the numerical simulation are visualised in Fig. 3. The

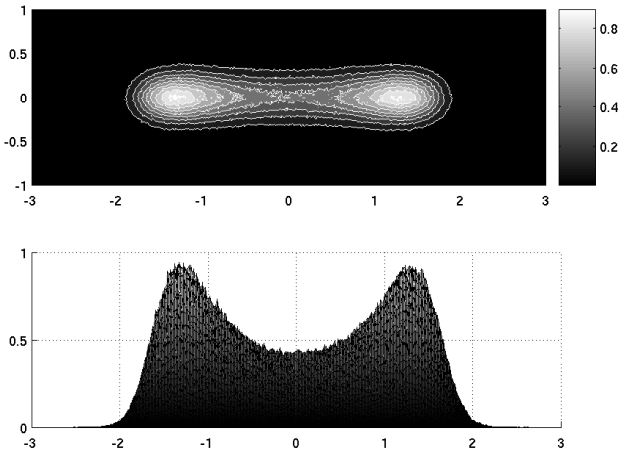

Figure 3: Steady state solution (i.e. invariant measure) of the microscopic equations (1.6).

cell migrates back and forth between the two chemoattractant sources. By the smallness of ε, the movement is like a relaxation oscillation, where the transition time between the sources is small compared to the time spent near the sources, which explains the two peaks in Fig. 3. In our simulations, cells never reached the boundary of the spatial domain.

Furthermore, the variance and covariance of the distribution of sensitivities is computed for every grid point the cell reaches within the domain. The results are visualised by plotting the cross-section $y = 1/120$ of the variance of the left-centred chemoattractant sensitivity and the covariance (Figure 4).

We use average values of these results to determine values for the (constant) covariance matrix in the macroscopic model

$$C = \begin{pmatrix} 0.54 & -0.36 \\ -0.36 & 0.54 \end{pmatrix}. \tag{5.1}$$

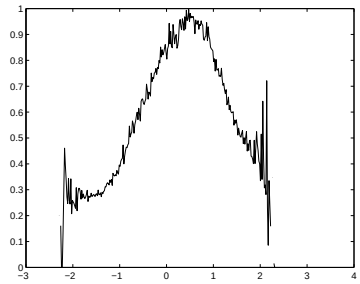

(a) Sample variances of the sensitivity for the chemoattractant centred at $(-2, 0)$.

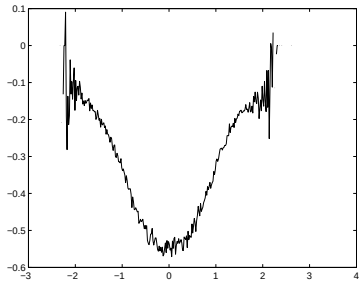

(b) Sample covariance of the sensitivities.

Figure 4: Variance and covariance as a function of x for $y = 1/120$.

As initial condition for the simulation of the macroscopic model we use an approximate δ-distribution in space centred at $(1, 0)$, so the initial condition is not symmetric but cells start near the second source of chemoattractant. Their initial sensitivities are given by $\hat{\chi}_i(S)$. We use von-Neumann boundary conditions.

The distribution of cells oscillates between the chemoattractant sources (Fig. 5) with amplitudes becoming smaller and smaller. Finally the solution approximates an equilibrium distribution (Fig. 6) which is similar to the equilibrium distribution obtained by direct simulation (Fig. 3).

Qualitatively the results for the steady states coincide, cells gather round the sources of chemoattractant and there is a certain fraction located in the centre. The difference between the microscopic solution and the macroscopic solution is displayed in Figure 7.

The equilibrium distribution of the direct simulation is higher than the one of the macroscopic equations near the sources of chemoattractants and lower in the centre of the domain.

These deviations can be explained by the fact, that we used constant average (co)variances as parameters in the macroscopic model equations. Actually the distributions of sensitivities depend on the cells' spatial positions, but these are not taken into account by the macroscopic model. Instead we overestimate the (co)variances close to the chemoattractant centres and underestimate them in the middle of the domain (see Figure 4 in comparison to the average values in matrix C in (5.1)).

We expect to find two groups of cells in the centre of the domain, one going to the right and one going to the left. By underestimating (Co)variances there, we introduce a smaller discrepancy of sensitivities between those to groups. This implies that the dominating sensitivity of all these cells is assumed to be lower which translates directly into lower migrational speed. But lower speed of cells in the centre of the domain implies that actually more cells are supposed to be located in that region.

The equilibrium density of the macroscopic equations is also lower close to the sources of chemoattractants (see Figure 7). In the direct simulations we

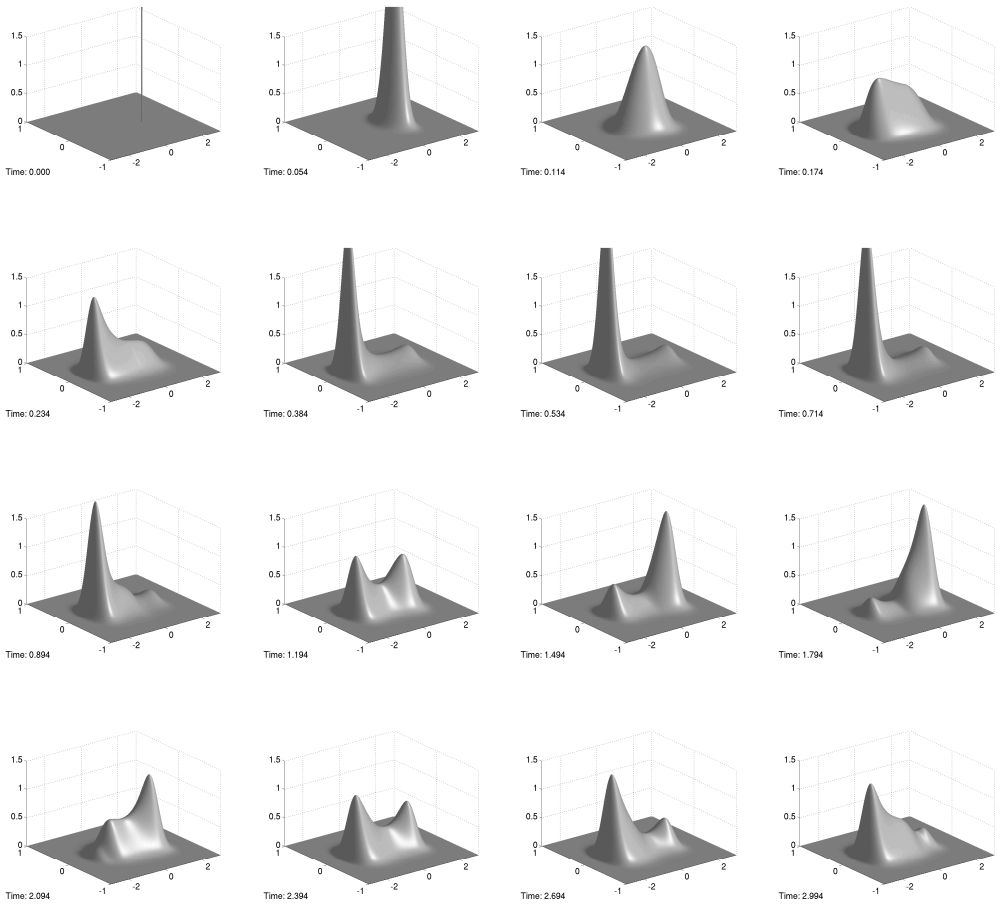

Figure 5: Time evolution of the leukocyte distribution.

observe that the distribution of cells is more pointed in this region and the distributions of their sensitivities are relatively thin compared to the rest of the domain (Figures 3, 4). By overestimating the (co)variances of their distributions of sensitivities, we allow cells to behave less uniformly and therefore to spread into a wider area.

Further numerical experiments showed that setting $c_{11} = c_{12} = c_{22} = c_{21} = 0$ fully inhibits convergence to equilibrium. Cells rather stay together and keep shuttling to and fro. Therefore the magnitude of the (co)variances seems to be related to the extent of desynchronisation and further to the "speed" of convergence to equilibrium whereas the frequency of oscillation between chemoattractant sources does not seem to be influenced.

6 Conclusion

In the parallel study [Oelz and Schmeiser 2004], simulations of the experiments in [Foxman, Campbell and Butcher 1997] are carried out and satisfactory quantitative agreement with the experimental results is achieved. These experiments and even more the later experimental publication [Foxman, Kunkel and Butcher 1999] focuses on the ability of the cells to undergo sequential chemotaxis to one at-

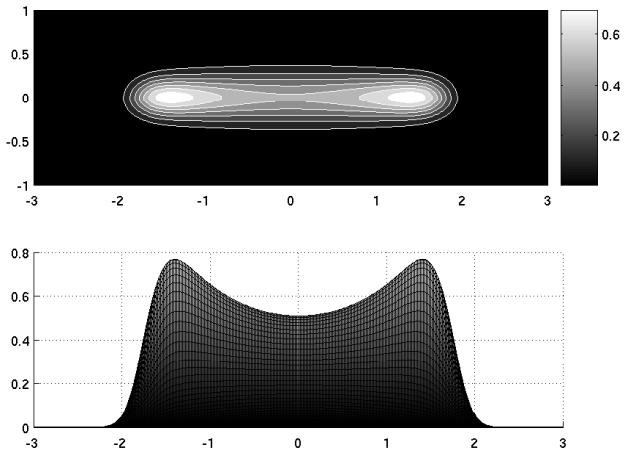

Figure 6: Steady state solution of the macroscopic model (3.2), (3.4).

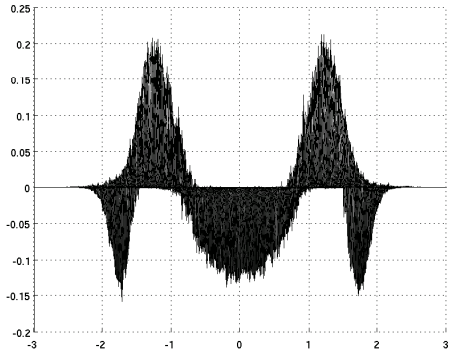

Figure 7: Difference (microscopic solution - macroscopic solution) between the two steady states as a function of x for $y = 0$.

tractant source after another and to be guided in a step-by-step fashion to their destinations within tissues. In fact, the results of Sections 2 and 5 reflect this behaviour, although restricted to the two-chemoattractant case. It might be possible to realise this situation in an experimental setting. One might establish stationary concentrations of two chemoattractants, centered at distant positions, by generating constant diffusive fluxes into the medium at the tips of two pipets and corresponding diffusive drainage fluxes using a permeable boundary membrane. In mathematical terms this would reproduce fundamental solutions of the Laplacian in contrast to the Gaussian profiles in (2.1). By performing time lapse video-microscopy as in fig. 1 long enough, one should be able to observe oscillations of single leukocytes between the sources of chemoattractants with characteristic frequency. We suggest to compare these to numerical results, either in order to estimate parameters or to validate the model.

List of Figures

References

[Foxman, Campbell and Butcher 1997] Foxman, E.F., Campbell, J.J., and Butcher, E.C., 1997, Multistep navigation and the combinatorial control of leukocyte chemotaxis. J. Cell Bio. **139**, 1349-1360

[Foxman, Kunkel and Butcher 1999] Foxman, E.F., Kunkel E.J., and Butcher, E.C., 1999, Integrating Conflicting Chemotactic Signals: The Role Of Memory in Leukocyte Navigation. J. Cell Bio. **147(3)**, 577-587

[Goldsby, Kindt, Osborne and Kuby 2000] Goldsby R.A., Kindt T.J., Osborne B.A. and Kuby J., Kuby Immunology 4. ed., New York, Freeman

[Guckenheimer and Holmes 1990] Guckenheimer J. and Holmes P, Nonlinear oscillations, dynamical systems, and bifurcations of vector fields., John F., Marsden J. E., Sirovich L., New York, Springer-Verlag

[Ionides, Fang, Isseroff and Oster 2004] Ionides E.L., Fang K.S., Isseroff R.R., Oster G.F., 2004, Stochastic models for cell motion and taxis. J. Math. Biol. **48**, 23-37

[Kloeden and Platen 1992] Kloeden P. E. and Platen E., Numerical solution of stochastic differential equations., Karatzas I. and Yor M., Berlin Heidelberg, Springer-Verlag

[Leveque 2002] Leveque, J. R., Finite Volume Methods for Hyperbolic Problems, Cambridge, Cambridge University Press

[Œksendal 1995] Œksendal, B.: Stochastic differential equations: An introduction with applications. 4.ed., Berlin Heidelberg, Springer-Verlag

[Painter, Maini and Othmer 2000] Painter K.J., Maini P.K., Othmer H.G., 2000, Development and applications of a model for cellular response to multiple chemotactic cues. J. Math. Biol. **41**, 285-314

[Oelz and Schmeiser 2004] Ölz D. B., Schmeiser C., 2004, Modelling of leukocyte chemotaxis and simulation of in-vitro experiments. Preprint